Progress In Electromagnetics Research B, Vol. 89, 111–132, 2020

Plane Wave Scattering by a PEC Half-Plane in Uniform Rectilinear Motion

Ramazan Daşbaşı and Burak Polat*

Abstract—Scattering of homogeneous plane waves by a Perfect Electric Conductor half-plane in uniform rectilinear motion in a simple lossless medium is investigated using Wiener-Hopf Technique in the context of Hertzian Electrodynamics. The cases of motion being parallel and perpendicular to the plane are tackled separately. Restrictions on incidence angle vs. speed for the realization of scattering phenomena are investigated in each case. Parallel motion mode reveals the possibility of excitation of surface waves upon reflection, which also contribute to edge diffraction mechanism. Numerical results are illustrated and discussed for scattered fields. Comparative theoretical results for the solution of the same problem using Special Relativity Theory are provided and discussed.

1. INTRODUCTION

Electromagnetic phenomena related to moving bodies that fall into the areas of application of Electrical Engineering are described by Hertzian Field Equations (HFEs), which were first introduced by Hertz in 1890 [1] and shaped into their final forms in modern vector algebraic notation by Heaviside in 1893 [2]. Descriptions of electromotive and magnetomotive forces (abbreviated as emf and mmf) in circuits in arbitrary motion and the linear Doppler Effect due to monochromatic sources in uniform rectilinear motion are two well-known features of HFEs with wide applications related to conversion and transmission of power in electromagnetic systems.

HFEs rest on Newtonian Continuum Mechanics in Euclidean Space and can be described as a projection of The Principle of Material Frame Indifference (PMFI) onto macroscopic electromagnetism. Hence, HFEs are tightly integrated with all disciplines of Continuum Mechanics that are formulated upon PMFI as well. PMFI has flourished in the works of Truesdell et al. [3, 4] starting by mid-20th century with ever-expanding theoretical capacity, experimental success, and engineering applications that also serve to unify disciplines of Continuum Mechanics. For a historic review and debates around the interpretations of PMFI and analogies between electromagnetic field and elastic continuum, the readers may refer to [5] and [6–9] (and the references cited therein), respectively.

The projection of PMFI onto macroscopic electromagnetism requires *frame indifference* of instantaneous values of emf and mmf induced around any closed contour as well as total electric and magnetic charges (fluxes) located in (leaving) any arbitrary volumetric domain. This has been demonstrated by Hertz employing the convective derivative operator $D_{\vec{\mathrm{v}}} = \partial_t + \vec{\mathrm{v}} \cdot \mathrm{grad}$ in the presence of bodies in general rectilinear motion with velocity field $\vec{\mathrm{v}}(t)$ and later extended by Heaviside for bodies with general velocity field $\vec{\mathrm{v}}(\vec{r}; t)$ by replacing the convective derivative operator with comoving time derivative operator $\partial_t + L_{\vec{\mathrm{v}}}$, where $L_{\vec{\mathrm{v}}}$ stands for the Lie derivative. The comoving time derivative operator is the only member of a family of invariant time derivatives (in the context of PMFI) which correctly models the well-known conservation laws in electromagnetism of moving bodies. It appears implicit in Reynolds and Helmholtz Transport Theorems in Vector Calculus for the special cases of

Received 10 June 2020, Accepted 26 October 2020, Scheduled 1 November 2020
* Corresponding author: Burak Polat (abpolat@yildiz.edu.tr).
The authors are with the Department of Electronics and Communications Engineering, Yildiz Technical University, Istanbul, Turkey.

scalar and vector fields. It is termed as *upper convected material derivative* in Elasticity and *Oldroyd derivative* [10] in Fluid Dynamics in the context of Tensor Calculus.

In 2010, one of the present authors succeeded to demonstrate the commutative property between the curl operator and the comoving time derivative operator when the velocity field is in its most general (nonsolenoidal and rotational) form, also covering non-Euclidean motion [11]. This development has been instrumental in obtaining the wave operator in its most general form and formulating numerous canonical radiation and scattering problems for bodies in various modes of motion accompanied by experimental verifications [12–17].

The present investigation is an application of Hertzian Electrodynamics to the canonical problem of uniform plane wave scattering by a Perfect Electric Conductor (PEC) half-plane in uniform rectilinear motion. We consider the scenario in Fig. 1, where a monochromatic plane wave impinges on a PEC half-plane S. The cases of motion of S being parallel and perpendicular to the plane are tackled separately.

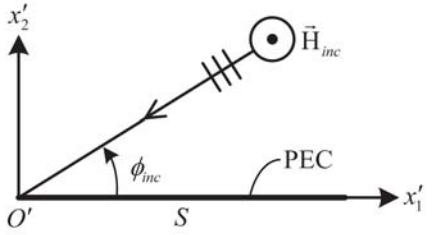

Figure 1. The geometry of the problem.

In virtue of the terminology of Continuum Mechanics, we use the term Eulerian frame (E-frame) for Cartesian spatial configuration $Ox_1x_2x_3t$, while material configuration $Ox_1'x_2'x_3't$, called Lagrangian or L-frame, signifies the Cartesian configuration of a material observer for which the half-plane is at rest, and ambient medium is in motion in opposite direction. The corresponding unit vectors along the coordinate axes lie in parallel: $\hat{x}_i = \hat{x}_i'$, $i = 1, 2, 3$.

The associated boundary value problem (BVP) is solved employing the following procedure:

(i) Map the incoming wave from E- to L-frame in virtue of kinematic transformations and Conservation Laws.

(ii) Solve the scattered wave from the associated BVP in L-frame which involves boundary, radiation, and edge conditions.

(iii) Map the scattered wave back from L- to E-frame.

This is followed by investigating the restrictions on incidence angle vs. speed for the realization of scattering phenomenon. Parallel motion mode reveals the possibility of excitation of surface waves upon reflection, which also contributes to edge diffraction mechanism. Numerical results are illustrated and discussed for scattered fields.

2. MOTION PARALLEL TO THE PLANE

2.1. Incoming Wave in E-Frame

Incident plane wave fields in E-frame satisfy the homogeneous Maxwell's equations of stationary media,

$$\begin{cases} \text{curl } \vec{E}_{inc}(\vec{r};t) + \partial_t \vec{B}_{inc}(\vec{r};t) = \vec{0} \\ \text{curl } \vec{H}_{inc}(\vec{r};t) - \partial_t \vec{D}_{inc}(\vec{r};t) = \vec{0} \\ \text{div } \vec{D}_{inc}(\vec{r};t) = 0 \\ \text{div } \vec{B}_{inc}(\vec{r};t) = 0 \end{cases}$$

in entire $\mathbb{R}_3$. In particular, we consider a uniform homogeneous TM plane wave with fields

$$\begin{cases} \vec{H}_{inc}(\vec{r};t) = \mathrm{Re}\left\{\vec{H}_{inc}(\vec{r})e^{-i\omega_{inc}t}\right\} = \hat{x}_3\,\mathrm{Re}\left\{u_{inc}(x_1,x_2)e^{-i\omega_{inc}t}\right\} \\ u_{inc}(x_1,x_2) = e^{ik\hat{n}_{inc}\cdot\vec{r}} = e^{-ik(x_1\cos\phi_{inc}+x_2\sin\phi_{inc})} \\ \vec{E}_{inc}(\vec{r};t) = Z\vec{H}_{inc}(\vec{r};t)\times\hat{n}_{inc} \end{cases} \tag{1}$$

impinging on a moving PEC half-plane described in L-frame at $S = \{(x_1', x_2', x_3')|\, x_1' > 0,\ x_2' = 0,\ x_3' \in (-\infty,\infty)\}$, as illustrated in Fig. 1.

The incoming fields satisfy the wave equations

$$\left(\mathrm{lap} - \frac{1}{c^2}\partial_t^2\right)\begin{pmatrix}\vec{E}_{inc}(\vec{r};t)\\ \vec{H}_{inc}(\vec{r};t)\end{pmatrix} = \vec{0}, \quad \left(\mathrm{lap} + k^2\right)\begin{pmatrix}\vec{E}_{inc}(\vec{r})\\ \vec{H}_{inc}(\vec{r})\end{pmatrix} = \vec{0}$$

in time and phasor domains, respectively. Here, $Z = \sqrt{\mu/\varepsilon}$ and $c = 1/\sqrt{\mu\varepsilon}$ are the characteristic impedance and the speed of light in the ambient simple lossless medium, while $\omega_{inc} > 0$ is the angular frequency, and $k = \omega_{inc}/c = 2\pi/\lambda$ represents the wave number.

We confine the incidence angle as $\phi_{inc} \in (0,\pi]$ due to the symmetric structure of the PEC half-plane. The scattering mechanism is investigated for the particular case of the velocity vector $\vec{\mathrm{v}} = \hat{x}_1 G$, $G = \mathrm{const.}$ with Galilean Transformations

$$x_1 = x_1' + Gt, \quad x_2 = x_2', \quad x_3 = x_3', \quad i = 1,2,3.$$

2.2. Incoming Wave in L-Frame

For L-observer, the PEC plane is at rest, and all material points in the ambient medium $\mathbb{R}_3\backslash S$ are in relative motion with velocity field

$$\vec{\mathrm{v}}' = -\vec{\mathrm{v}}\cdot\bar{\bar{I}} = -\hat{x}_1' G,$$

where $\bar{\bar{I}} = \hat{x}_1\hat{x}_1' + \hat{x}_2\hat{x}_2' + \hat{x}_3\hat{x}_3'$ is the unit dyadic. In L-frame, the incident fields satisfy the time domain Hertzian field and wave equations

$$\begin{cases} \mathrm{curl}'\,\vec{E}_{inc}'(\vec{r}';t) + (\partial_t + L_{\vec{\mathrm{v}}'})\vec{B}_{inc}'(\vec{r}';t) = \vec{0} \\ \mathrm{curl}'\,\vec{H}_{inc}'(\vec{r}';t) - (\partial_t + L_{\vec{\mathrm{v}}'})\vec{D}_{inc}'(\vec{r}';t) = \vec{0} \\ \mathrm{div}'\,\vec{D}_{inc}'(\vec{r}';t) = 0 \\ \mathrm{div}'\,\vec{B}_{inc}'(\vec{r}';t) = 0 \end{cases} \tag{2a-d}$$

$$\begin{cases} L_{\vec{\mathrm{v}}'}\vec{B}_{inc}' = \vec{\mathrm{v}}'\ \mathrm{div}'\,\vec{B}_{inc}' - \mathrm{curl}'(\vec{\mathrm{v}}'\times\vec{B}_{inc}') = -\,\mathrm{curl}'(\vec{\mathrm{v}}'\times\vec{B}_{inc}') \\ L_{\vec{\mathrm{v}}'}\vec{D}_{inc}' = \vec{\mathrm{v}}'\ \mathrm{div}'\,\vec{D}_{inc}' - \mathrm{curl}'(\vec{\mathrm{v}}'\times\vec{D}_{inc}') = -\,\mathrm{curl}'(\vec{\mathrm{v}}'\times\vec{D}_{inc}') \end{cases} \tag{2e-f}$$

$$\left(\mathrm{lap}' - \frac{1}{c^2}\left(\partial_t + L_{\vec{\mathrm{v}}'}\right)^2\right)\begin{pmatrix}\vec{E}_{inc}'(\vec{r}';t)\\ \vec{H}_{inc}'(\vec{r}';t)\end{pmatrix} = \vec{0}, \quad \vec{r}' \in \mathbb{R}_3. \tag{3}$$

Here, $L_{\vec{\mathrm{v}}'}$ represents the Lie derivative operator. The projection of Eqs. (2a-d) and (3) into phasor domain reads

$$\begin{cases} \mathrm{curl}'\ \vec{E}_{inc}'(\vec{r}) - i\omega_{inc}\vec{B}_{inc}'(\vec{r}') = \vec{0} \\ \mathrm{curl}'\ \vec{H}_{inc}'(\vec{r}') + i\omega_{inc}\vec{D}_{inc}'(\vec{r}') = \vec{0} \\ \mathrm{div}'\ \vec{D}_{inc}'(\vec{r}') = 0 \\ \mathrm{div}'\ \vec{B}_{inc}'(\vec{r}') = 0 \end{cases}$$

and

$$\left(\mathrm{lap}' + k^2\right)\begin{pmatrix}\vec{E}_{inc}'(\vec{r}')\\ \vec{H}_{inc}'(\vec{r}')\end{pmatrix} = \vec{0}, \quad \vec{r}' \in \mathbb{R}_3$$

in virtue of *invariance of wavenumber* in E- and L-frames (cf. [11], Sect. 7). PMFI requires the field transformations

$$\begin{cases} \vec{E}'_{inc} = \vec{E}_{inc} \cdot \bar{\bar{I}}, & \vec{H}'_{inc} = \vec{H}_{inc} \cdot \bar{\bar{I}} \\ \vec{D}'_{inc} = \vec{D}_{inc} \cdot \bar{\bar{I}}, & \vec{B}'_{inc} = \vec{B}_{inc} \cdot \bar{\bar{I}} \end{cases}$$

The incoming fields in the two frames also satisfy

$$\begin{cases} \operatorname{curl}' \vec{E}'_{inc} = \operatorname{curl} \vec{E}_{inc} \cdot \bar{\bar{I}} \\ \operatorname{curl}' \vec{H}'_{inc} = \operatorname{curl} \vec{H}_{inc} \cdot \bar{\bar{I}} \end{cases} \quad \text{and} \quad \begin{cases} \partial_t \vec{B}_{inc} = (\partial_t + L_{\vec{\mathrm{v}}'}) \vec{B}'_{inc} \cdot \bar{\bar{I}} \\ \partial_t \vec{D}_{inc} = (\partial_t + L_{\vec{\mathrm{v}}'}) \vec{D}'_{inc} \cdot \bar{\bar{I}} \end{cases} .$$

Accordingly, the map of the incoming wave in Eq. (1) into L-frame is derived as

$$\begin{cases} \vec{H}'_{inc}(\vec{r}\,';t) = \hat{x}'_3 \operatorname{Re}\left\{ u'_{inc}(x'_1, x'_2) e^{-i\omega'_{inc} t} \right\} \\ u'_{inc}(x'_1, x'_2) = e^{ik\hat{n}'_{inc} \cdot \vec{r}\,'} = e^{-ik\left(x'_1 \cos\phi_{inc} + x'_2 \sin\phi_{inc}\right)} \\ \vec{E}'_{inc}(\vec{r}\,';t) = Z \vec{H}'_{inc}(\vec{r}\,';t) \times \hat{n}'_{inc} \end{cases}$$

with $\omega'_{inc} = \omega_{inc}(1 + \beta \cos\phi_{inc})$, $\beta = G/c$.

In L-frame, the incoming wave is also observed as a homogeneous monochromatic plane wave with the kinematic limitation $(1 + \beta \cos\phi_{inc}) > 0$ on (ϕ_{inc}, β) for the incident wave to catch the moving half-plane.

2.3. The Representation of Scattered Wave in L-Frame

Based on Superposition Principle, let us express the total field in the ambient medium as

$$\begin{cases} \left(\vec{E}_{tot}, \vec{H}_{tot}\right) = \left(\vec{E}_{inc}, \vec{H}_{inc}\right) + \left(\vec{E}_{sc}, \vec{H}_{sc}\right) \\ \left(\vec{E}'_{tot}, \vec{H}'_{tot}\right) = \left(\vec{E}'_{inc}, \vec{H}'_{inc}\right) + \left(\vec{E}'_{sc}, \vec{H}'_{sc}\right) \end{cases}$$

in spatial and material configurations, respectively. The problem under consideration further allows us to express the total scattered fields as a combination of reflected and diffracted components, namely,

$$\begin{cases} \left(\vec{E}_{sc}, \vec{H}_{sc}\right) = \left(\vec{E}_{ref}, \vec{H}_{ref}\right) + \left(\vec{E}_{d}, \vec{H}_{d}\right) \\ \left(\vec{E}'_{sc}, \vec{H}'_{sc}\right) = \left(\vec{E}'_{ref}, \vec{H}'_{ref}\right) + \left(\vec{E}'_{d}, \vec{H}'_{d}\right) \end{cases}$$

which satisfy the same set of field and wave equations as the total scattered fields in respective frames.

2.4. Scattered Wave for L-Observer Located on S

For an L-observer located on S, all material points in the ambient medium $\mathbb{R}_3 \backslash S$ move with velocity $\vec{\mathrm{v}}'$, and the corresponding scattering mechanism is characterized by

$$\begin{cases} \operatorname{curl}' \vec{E}'_{sc}(\vec{r}\,';t) + (\partial_t + L_{\vec{\mathrm{v}}'}) \vec{B}'_{sc}(\vec{r}\,';t) = \vec{0} \\ \operatorname{curl}' \vec{H}'_{sc}(\vec{r}\,';t) - (\partial_t + L_{\vec{\mathrm{v}}'}) \vec{D}'_{sc}(\vec{r}\,';t) = \vec{0} \\ \operatorname{div}' \vec{D}'_{sc}(\vec{r}\,';t) = 0 \\ \operatorname{div}' \vec{B}'_{sc}(\vec{r}\,';t) = 0 \end{cases} \tag{4a-d}$$

$$\begin{cases} L_{\vec{\mathrm{v}}'} \vec{B}'_{sc} = \vec{\mathrm{v}}' \operatorname{div}' \vec{B}'_{sc} - \operatorname{curl}'(\vec{\mathrm{v}}' \times \vec{B}'_{sc}) = -\operatorname{curl}'(\vec{\mathrm{v}}' \times \vec{B}'_{sc}) \\ L_{\vec{\mathrm{v}}'} \vec{D}'_{sc} = \vec{\mathrm{v}}' \operatorname{div}' \vec{D}'_{sc} - \operatorname{curl}'(\vec{\mathrm{v}}' \times \vec{D}'_{sc}) = -\operatorname{curl}'(\vec{\mathrm{v}}' \times \vec{D}'_{sc}) \end{cases} \tag{4e-f}$$

$$\left(\operatorname{lap}' - \frac{1}{c^2} (\partial_t + L_{\vec{\mathrm{v}}'})^2 \right) \begin{pmatrix} \vec{E}'_{sc}(\vec{r}\,';t) \\ \vec{H}'_{sc}(\vec{r}\,';t) \end{pmatrix} = \vec{0}, \quad \vec{r}\,' \in \mathbb{R}_3 \backslash S. \tag{5}$$

Accordingly, Eqs. (4a) and (4b) can also be expressed in the form

$$\begin{cases} \operatorname{curl}'\left(\vec{E}'_{sc} - \vec{\mathrm{v}}' \times \vec{B}'_{sc}\right) + \partial_t \vec{B}'_{sc} = \vec{0} \\ \operatorname{curl}'\left(\vec{H}'_{sc} + \vec{\mathrm{v}}' \times \vec{D}'_{sc}\right) - \partial_t \vec{D}'_{sc} = \vec{0}. \end{cases}$$

In the present problem, the volume (free) charge and conduction current density distributions are available only on S and described by

$$\rho'_f(\vec{r}';t) = \rho'_S(x'_1;t)\,\delta(x'_2)\,U(x'_1), \quad \vec{J}'_C(\vec{r}';t) = \hat{x}'_1 J'_S(x'_1;t)\,\delta(x'_2)\,U(x'_1) \tag{6a}$$

with $\delta(\cdot)$ and $U(\cdot)$ representing the Dirac Delta distribution and Unit Step function, respectively. The Principle of Continuity of Current reads

$$\operatorname{div}' \vec{J}'_C(\vec{r}';t) + \partial_t \rho'_f(\vec{r}';t) = 0 \tag{6b}$$

and applied in the sense of distributions. The boundary relations on S are obtained from the distributional investigations of Eqs. (4)–(6) as $\vec{\mathrm{v}}' \to \vec{0}$. Obviously, the boundary relations on S correspond to the same result as those for Maxwell's equations of stationary media,

$$\begin{cases} \hat{x}'_2 \times \left[\vec{E}'_{sc}(\vec{r}';t)\big|_{S^+} - \vec{E}'_{sc}(\vec{r}';t)\big|_{S^-}\right] = \vec{0} \\ \hat{x}'_2 \times \left[\vec{H}'_{sc}(\vec{r}';t)\big|_{S^+} - \vec{H}'_{sc}(\vec{r}';t)\big|_{S^-}\right] = \vec{J}'_S(\vec{r}'_S;t) \\ \hat{x}'_2 \cdot \left[\vec{D}'_{sc}(\vec{r}';t)\big|_{S^+} - \vec{D}'_{sc}(\vec{r}';t)\big|_{S^-}\right] = \rho'_S(\vec{r}'_S;t) \\ \hat{x}'_2 \cdot \left[\vec{B}'_{sc}(\vec{r}';t)\big|_{S^+} - \vec{B}'_{sc}(\vec{r}';t)\big|_{S^-}\right] = 0 \end{cases} \tag{7a-d}$$

The boundary relations are accompanied by the description of a stationary PEC body

$$\hat{x}'_2 \times \left[\vec{E}'_{inc}(\vec{r}';t) + \vec{E}'_{sc}(\vec{r}';t)\right]\Big|_S = \vec{0}, \tag{7e}$$

the edge condition as $\rho' = \sqrt{x'^2_1 + x'^2_2} \to 0$ and the radiation condition as $\rho' \to \infty$. In Eq. (7), $S^{\pm}$ denote half-planes that are parallel and infinitely close to S when one approaches as $x_2 \to 0^+$ and $x_2 \to 0^-$.

2.5. Scattered Wave for L-Observer Located in $\mathbb{R}_3 \backslash S$

For an L-observer (located at a fixed point) in $\mathbb{R}_3 \backslash S$, the body S and therefore all material points in the ambient medium move with velocity $-\vec{\mathrm{v}}'$. Then, the corresponding scattering mechanism is characterized by

$$\begin{cases} \operatorname{curl}'\left(\vec{E}'_{sc} + \vec{\mathrm{v}}' \times \vec{B}'_{sc}\right) + \partial_t \vec{B}'_{sc} = \vec{0} \\ \operatorname{curl}'\left(\vec{H}'_{sc} - \vec{\mathrm{v}}' \times \vec{D}'_{sc}\right) - \partial_t \vec{D}'_{sc} = \vec{J}'_C + \vec{J}_{-\vec{\mathrm{v}}'} \\ \operatorname{div}' \vec{D}'_{sc} = \rho'_f \\ \operatorname{div}' \vec{B}'_{sc} = 0 \end{cases}$$

$$\operatorname{div}'\left(\vec{J}'_C(\vec{r}';t) + \vec{J}_{-\vec{\mathrm{v}}'}(\vec{r}';t)\right) + \partial_t \rho'_f(\vec{r}';t) = 0$$

$$\left(\operatorname{lap}' - \frac{1}{c^2}(\partial_t + L_{-\vec{\mathrm{v}}'})^2\right) \begin{pmatrix} \vec{E}'_{sc}(\vec{r}';t) \\ \vec{H}'_{sc}(\vec{r}';t) \end{pmatrix} = \vec{0}, \quad \vec{r}' \in \mathbb{R}_3 \backslash S \tag{8}$$

with $\vec{J}_{-\vec{\mathrm{v}}'} = -\vec{\mathrm{v}}' \rho'_f$ corresponding to convection currents on S. The special case of monochromatic incidence requires that all field quantities related to the scattered wave in L-frame are also

monochromatic with time dependence $\exp(-i\omega'_{sc}t)$. Then, the phasor fields, as observed in $\mathbb{R}_3\backslash S$ in L-frame, satisfy the reduced field and wave equations

$$\begin{cases} \operatorname{curl}' \vec{E}'_{sc}(\vec{r}') - i\omega_{inc}\vec{B}'_{sc}(\vec{r}') = \vec{0} \\ \operatorname{curl}' \vec{H}'_{sc}(\vec{r}') + i\omega_{inc}\vec{D}'_{sc}(\vec{r}') = \vec{J}'_C(\vec{r}') + \vec{J}_{-\vec{v}'}(\vec{r}') \\ \operatorname{div}' \vec{D}'_{sc}(\vec{r}') = \rho'_f(\vec{r}') \\ \operatorname{div}' \vec{B}'_{sc}(\vec{r}') = 0 \end{cases} \tag{9a-d}$$

$$\operatorname{div}' \left(\vec{J}'_C(\vec{r}') + \vec{J}_{-\vec{v}'}(\vec{r}') \right) - i\omega_{inc}\, \rho'_f(\vec{r}') = 0 \tag{9e}$$

$$\left(\operatorname{lap}' + k^2\right) \begin{pmatrix} \vec{E}'_{sc}(\vec{r}') \\ \vec{H}'_{sc}(\vec{r}') \end{pmatrix} = \vec{0}, \quad \vec{r}' \in \mathbb{R}_3\backslash S. \tag{10}$$

In what follows we shall continue with the solution of the reflected components in the first place.

2.6. Reflected Wave in L-Frame

In calculating the reflected wave, we consider a PEC plane of *infinite extent* located on $x'_2 = 0$. Then, the reflected fields can be expressed in the form

$$\begin{cases} \vec{H}'_{ref}(\vec{r}';t) = \hat{x}'_3 \operatorname{Re}\left\{ u'_{ref}(x'_1, x'_2) e^{-i\omega'_{ref}t} \right\} \\ u'_{ref}(x'_1, x'_2) = R_{TM} e^{ik\hat{n}'_{ref}\cdot\vec{r}'} = R_{TM} e^{ik\left(x'_1 \cos\phi_{ref} + x'_2 \sin\phi_{ref}\right)} \\ \vec{E}'_{ref}(\vec{r}';t) = Z\vec{H}'_{ref}(\vec{r}';t) \times \hat{n}'_{ref} \end{cases} \tag{11a-c}$$

Notice that we switch from the general notation ω'_{sc} to ω'_{ref} as the present geometry allows for geometrical optics (GO) (i.e., space wave) fields. The unknown quantities in Eq. (11) are solved from the BVP

$$\begin{cases} \left(\operatorname{lap}' - \dfrac{1}{c^2} \left(\partial_t + L_{-\vec{v}'}\right)^2 \right) \vec{E}'_{ref}\left(x'_1, x'_2; t\right), \quad x'_2 > 0 \\ \hat{x}'_2 \times \left[\vec{E}'_{inc}\left(x'_1, 0; t\right) + \vec{E}'_{ref}\left(x'_1, 0; t\right) \right] = \vec{0} \\ \lim\limits_{|\vec{r}'|\to\infty} \left(\vec{E}'_{ref} \times \vec{r}' + |\vec{r}'|\ \vec{H}'_{ref} \right) = \vec{0}, \quad x'_2 > 0 \end{cases} \tag{12a-c}$$

for $x'_1 \in (-\infty, \infty)$, $\forall t$. It uniquely reads the Snell's Law for parallel motion,

$$\cos\phi_{ref} = -\cos\phi_{inc}/(1 + 2\beta\cos\phi_{inc}) = \cos\phi^0_{ref}/(1 + 2\beta\cos\phi_{inc}) \tag{13a}$$

with $\phi^0_{ref} = \pi - \phi_{inc}$ denoting the angle of reflection in the stationary case $\beta = 0$, and

$$\omega'_{ref} = \omega_{inc}(1 + \beta\cos\phi_{ref}) = \omega_{inc}\frac{(1 + \beta\cos\phi_{inc})}{(1 + 2\beta\cos\phi_{inc})} \tag{13b}$$

$$R_{TM} = \sin\phi_{inc}/\sin\phi_{ref} \tag{13c}$$

We observe the condition

$$\omega'_{ref} > 0; \quad \text{i.e.,} \quad \frac{1 + \beta\cos\phi_{inc}}{1 + 2\beta\cos\phi_{inc}} > 0$$

as a second kinematic requirement on (ϕ_{inc}, β) for the realization of wave reflection phenomenon.

In TE mode, the angle and frequency of the reflected wave are the same as those in TM mode, while full reflection is observed: $R_{TE} = -1$.

2.7. Reflected Wave in E-Frame

The maps of $(\vec{E}'_{ref}, \vec{H}'_{ref})$ into E-frame read

$$\begin{cases} \vec{H}_{ref}(\vec{r};t) = \vec{H}'_{ref}(\vec{r}';t)\cdot\bar{\bar{I}} = \hat{x}_3\,\mathrm{Re}\left\{u_{ref}(x_1,x_2)e^{-i\omega_{ref}t}\right\} \\ u_{ref}(x_1,x_2) = R_{TM}e^{ik\hat{n}_{ref}\cdot\vec{r}} = R_{TM}e^{ik(x_1\cos\phi_{ref}+x_2\sin\phi_{ref})} \\ \vec{E}_{ref}(\vec{r};t) = Z\vec{H}_{ref}(\vec{r};t)\times\hat{n}_{ref} \end{cases}$$

with

$$\omega_{ref} = \omega_{inc}(1+2\beta\cos\phi_{ref}) = \omega_{inc}/(1+2\beta\cos\phi_{inc}) \tag{14}$$

Equation (14) reveals the well-known Doppler Effect due to the component of the incident wave parallel to the direction of motion. When we express the angular frequency of the reflected wave as $\omega_{ref} = \omega_{inc} + \Delta\omega$, we get

$$\Delta\omega/\omega_{inc} = -2\beta\cos\phi_{inc}/(1+2\beta\cos\phi_{inc})$$

The third kinematic requirement on (ϕ_{inc}, β) for the realization of wave reflection phenomenon appears as

$$\omega'_{ref} > 0; \quad \text{i.e.,} \quad \frac{1+\beta\cos\phi_{inc}}{1+2\beta\cos\phi_{inc}} > 0$$

One observes that $\Delta\omega \le 0$ when $\beta\cos\phi_{inc} \ge 0$, i.e., when $\phi_{inc} \in (0,\pi/2]$, $\beta > 0$ or $\phi_{inc} \in (\pi/2,\pi]$, $\beta < 0$. Similarly, $\Delta\omega \ge 0$ when $\beta\cos\phi_{inc} \le 0$, i.e., when $\phi_{inc} \in (0,\pi/2]$, $\beta < 0$ or $\phi_{inc} \in (\pi/2,\pi]$, $\beta > 0$.

For both TM and TE modes, the parallel motion of the plane has no influence on the reflected wave under normal incidence $\phi_{inc} = \pi/2$.

It might also be interesting to acknowledge the asymptotic case $\beta \to \infty$, which reads

$$\phi_{ref} \to \pi/2, \quad R_{TM} \to \sin\phi_{inc}, \quad \omega'_{ref} \to \omega_{inc}/2, \quad \omega_{ref} \to 0$$

while $\phi_{inc} \neq \pi/2$.

2.8. Dependence of Wave Mechanism on (ϕ_{inc}, β)

Let us outline the three conditions on (ϕ_{inc}, β) which we have obtained so far for the realization of scattering phenomenon:

$$\begin{cases} \text{Condition I}: & 1+\beta\cos\phi_{inc} > 0 \\ \text{Condition II}: & \dfrac{1+\beta\cos\phi_{inc}}{1+2\beta\cos\phi_{inc}} > 0 \\ \text{Condition III}: & 1+2\beta\cos\phi_{inc} > 0 \end{cases}$$

We observe the following:

- Condition I is satisfied when Condition III is satisfied.
- Condition II is satisfied when Conditions I and III are satisfied.

Therefore, Condition III appears sufficient for the other two conditions to hold. Condition III holds for $\forall\phi_{inc} \in (0,\pi]$ when $|\beta| < 1/2$, while it requires $\phi_{inc} \in \left[\cos^{-1}(1/2|\beta|,\pi\right]$ and $\phi_{inc} \in \left(0, \pi - \cos^{-1}(1/2\beta)\right)$ for $\beta \le -1/2$ and $\beta \ge 1/2$, respectively, as illustrated in Fig. 2. The wave reflection mechanism takes place for $\forall\beta$ when

$$\phi_{inc} \in \left(\cos^{-1}\left(1/2\,|\beta|\right), \pi - \cos^{-1}\left(1/2\,|\beta|\right)\right)$$

Condition III addresses a certain permissible region in (ϕ_{inc}, β) plane where wave propagation and reflection phenomena are observed. This region comprises sub-regions separated by the boundary curves

$$|\cos\phi_{ref}| = |\cos\phi_{inc}|/|1+2\beta\cos\phi_{inc}|$$

determined by Snell's Law in Eq. (13a). These adjoining domains are specified as $|\cos\phi_{ref}| \le 1$ and $|\cos\phi_{ref}| > 1$ for which the reflected wave appears as space wave and surface wave, respectively, as plotted in Fig. 3.

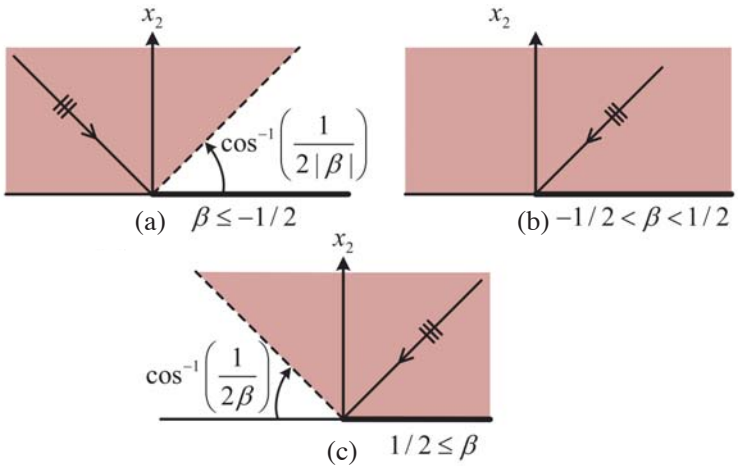

Figure 2. Variations of (painted) ranges of ϕ_{inc} with β in which wave phenomena is realized for uniform motion parallel to the plane.

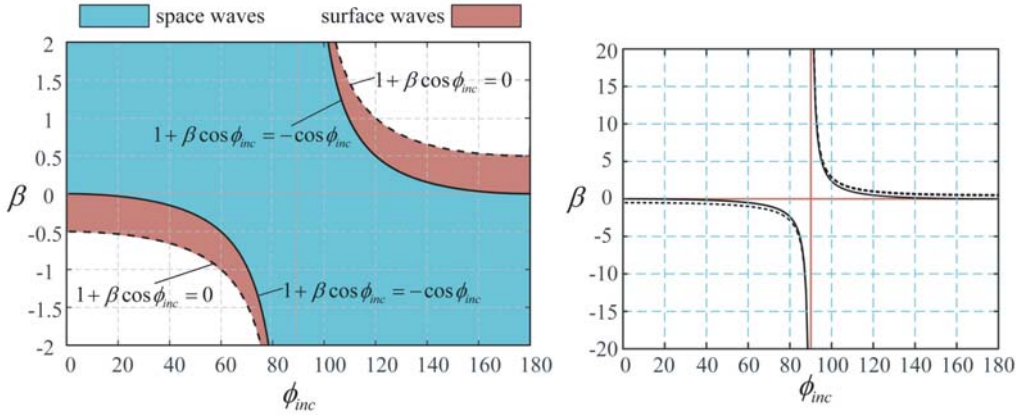

Figure 3. Computations of permissible regions in (ϕ_{inc}, β) that denote space and surface wave mechanisms in two different scales.

Space wave reflection mechanism can be described w.r.t. β as

$$\begin{cases} \phi_{ref} > \phi^0_{ref} = \pi - \phi_{inc}; \quad \omega_{ref} > \omega_{inc}; \quad R_{TM} > 1 \quad \text{for } \beta < 0 \\ \phi_{ref} < \phi^0_{ref}; \quad \omega_{ref} < \omega_{inc}; \quad R_{TM} < 1 \quad \text{for } \beta > 0 \end{cases}$$

and is illustrated in Fig. 4 for $\phi_{inc} \in (0, \pi/2]$.

The surface wave excitation mechanism illustrated in Fig. 5 requires to introduce

$$\sin\phi_{ref} = \sqrt{1 - \cos^2\phi_{ref}} = iN \tag{15a}$$

with $N = \sqrt{\cos^2\phi_{ref} - 1} > 0$ so that exponential decay of the reflected field

$$u'_{ref}(x'_1, x'_2) = R_{TM} e^{ikx'_1 \cos\phi_{ref}} e^{-kNx'_2} \tag{15b}$$

is provided in the upper half-space $x'_1 \in (-\infty, \infty)$, $x'_2 > 0$. Substituting $\phi_{ref} = \mathrm{Re}\{\phi_{ref}\} + i\,\mathrm{Im}\{\phi_{ref}\}$ into Eq. (15a) and using the identity $\sin(a+ib) = \sin(a)\cosh(b) + i\cos(a)\sinh(b)$, the reflection angle can be located on positive imaginary axis at

$$\phi_{ref} = i \sinh^{-1} N. \tag{15c}$$

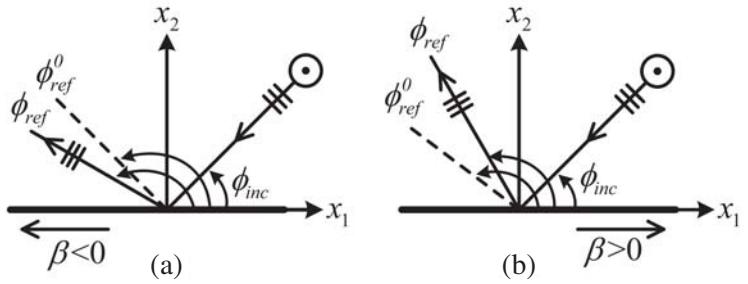

Figure 4. Illustration of space wave reflection mechanism for opposite directions of uniform motion parallel to the plane.

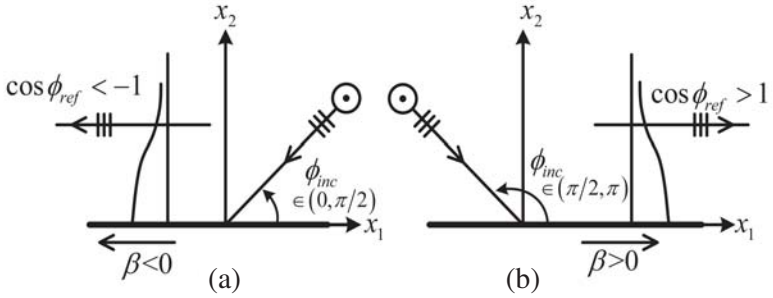

Figure 5. Illustration of surface wave reflection mechanism for opposite directions of uniform motion parallel to the plane.

2.9. Surface Wave Reflection for Very Small Values of β

In Table 1, we scrutinize surface wave reflection mechanism for certain vehicles of practical importance. Since the corresponding β values are quite small, it is seen that surface waves (falling into the red regions in Fig. 3) occur only for grazing incidence $\phi_{inc} \to 0, \pi$. In this case, we may introduce the asymptotic representation of Snell's Law in Eq. (13a),

$$\begin{aligned} cos\phi_{ref} &= -\cos\phi_{inc}\left(1-2\beta\cos\phi_{inc}\right)+\text{h.o.t. in }\beta \\ &\to \mp\left(1+2\left|\beta\right|\right)+\text{h.o.t. in }\left|\beta\right|, \quad \phi_{inc}\to 0,\pi \\ \sin\phi_{ref} &= i\sqrt{\cos^2\phi_{ref}-1} = i\sqrt{\cos^2\phi_{inc}\left(1-4\beta\cos\phi_{inc}\right)-1+\text{h.o.t. in }\beta} \\ &\to i\sqrt{4\left|\beta\right|+\text{h.o.t. in }\left|\beta\right|}, \quad \phi_{inc}\to 0,\pi \end{aligned}$$

Table 1. Constraints on the angle of incidence w.r.t.? typical speeds for surface wave reflection mechanism.

Vehicle	**Typical Speeds G vs. β**	**Ranges of ϕ_{inc}**
International Space Station	$G = 7660$ [m/s], $\beta = \pm 2.55\text{e}-5$	$\phi_{inc} \in (0°, 0.41°) \cup (179.59°, 180°)$
Military Jet Plane	$G = 1200$ [m/s], $\beta = \pm 4\text{e}-6$	$\phi_{inc} \in (0°, 0.16°) \cup (179.84°, 180°)$
Ballistic Missile	$G = 5000$ [m/s], $\beta = \pm 1.67\text{e}-5$	$\phi_{inc} \in (0°, 0.33°) \cup (179.67°, 180°)$
Commercial Airplane	$G = 260$ [m/s], $\beta = \pm 8.67\text{e}-7$	$\phi_{inc} \in (0°, 0.07°) \cup (179.93°, 180°)$

and place into the constituents of surface reflected wave in Eq. (15b) as

$$R_{TM} = \left.\frac{\sin\phi_{inc}}{\sin\phi_{ref}}\right|_{\phi_{inc}\to 0,\pi} \to \frac{\sin\phi_{inc}}{i\sqrt{4\,|\beta| + \text{h.o.t. in } |\beta|}}$$

$$\left. e^{ikx_1'\cos\phi_{ref}}\right|_{\phi_{inc}\to 0,\pi} \to e^{\mp i(1+2|\beta|+\text{h.o.t. in } |\beta|)kx_1'}$$

$$\left. e^{-kx_2'\sqrt{\cos^2\phi_{ref}-1}}\right|_{\phi_{inc}\to 0,\pi} \to e^{-kx_2'\sqrt{4|\beta|+\text{h.o.t. in } |\beta|}}$$

to observe that the surface reflected wave behaves like

$$u_{ref}'(x_1',x_2')\big|_{\phi_{inc}\to 0,\pi} \to \frac{\sin\phi_{inc}}{i2\sqrt{|\beta|}}\, e^{-2\sqrt{|\beta|}kx_2'}\, e^{\mp i(1+2|\beta|)kx_1'}$$

under a first order approximation in β. It may be realized that the amplitude $\sin\phi_{inc}/(2\sqrt{|\beta|})$ does not necessarily take small values while the exponential decay along x_2'-axis is quite slow.

2.10. Far Field Scattered Wave in L-Frame

The scattered wave in L-frame is solved from Eq. (8) under the boundary conditions (7a-d), (12b), the edge condition as $\rho' = \sqrt{{x_1'}^2 + {x_2'}^2} \to 0$, and the radiation condition as $\rho' \to \infty$. First, we incorporate Eq. (12b) into Eq. (7c) as

$$\hat{x}_2' \times \left[-\vec{E}_{ref}'(\vec{r}\,';t) + \vec{E}_{sc}'(\vec{r}\,';t)\right]\Big|_S = \vec{0}.$$

Then, by setting

$$\begin{cases} \vec{H}_{sc}'(\vec{r}\,';t) = \hat{x}_3'\text{Re}\left\{u'(x_1',x_2')e^{-i\omega_{ref}'t}\right\} \\ \vec{H}_d'(\vec{r}\,';t) = \hat{x}_3'\text{Re}\left\{u_d'(x_1',x_2')e^{-i\omega_{ref}'t}\right\} \\ \vec{J}_S'(\vec{r}\,'_S;t) = \hat{x}_1'\text{Re}\left\{J_S'(x_1')e^{-i\omega_{ref}'t}\right\} \end{cases}$$

the associated reduced BVP is constructed on Helmholtz Equation (9) as

$$\begin{cases} (\text{lap}' + k^2)\,u'(x_1',x_2') = 0, \quad (x_1',x_2') \notin S \\ \dfrac{\partial}{\partial x_2'}u'(x_1',0) = ik\sin\phi_{ref}R_{TM}e^{ikx_1'\cos\phi_{ref}}, \quad x_1' > 0 \\ \dfrac{\partial}{\partial x_2'}u'(x_1',+0) - \frac{\partial}{\partial x_2'}u'(x_1',-0) = 0, \quad x' > 0 \\ u'(x_1',+0) - u'(x_1',-0) = J_S'(x_1'), \quad x_1' > 0 \\ u'(x_1',+0) - u'(x_1',-0) = 0, \quad x_1' < 0 \\ \dfrac{\partial}{\partial x_2'}u'(x_1',+0) - \frac{\partial}{\partial x_2'}u'(x_1',-0) = 0, \quad x_1' < 0 \\ u'(x_1',0) = O(1), \quad \dfrac{\partial}{\partial x_2'}u'(x_1',0) = O(|x_1'|^{-1/2}), \quad x_1' \to 0 \\ u'(x_1',0) = O(e^{-ikx_1'}), \quad x_1' \to -\infty \\ u'(x_1',0) = O(e^{-ikx_1'\cos\phi_{ref}}), \quad x_1' \to \infty \end{cases} \tag{16}$$

It may be realized that the BVP in Eq. (16) is similar to the one for the stationary case, and they coincide when one substitutes

$$R_{TM} \to 1, \quad \phi_{ref} \to \phi_{ref}^0 = \pi - \phi_{inc} \;\text{ for }\; \beta = 0.$$

Therefore, a solution can be obtained directly by proper substitutions in the result available in literature [18] through Wiener-Hopf Technique for the stationary case as

$$u'(\rho',\phi') = \begin{cases} \dfrac{1}{2\pi i} R_{TM}\sqrt{1-\cos\phi_{ref}} \displaystyle\int_{\Gamma} \frac{e^{ik\rho'\cos(\phi'-t)}\sqrt{1+\cos t}}{\cos t-\cos\phi_{ref}}dt, & \phi' \in (0,\pi) \\ -\dfrac{1}{2\pi i} R_{TM}\sqrt{1-\cos\phi_{ref}} \displaystyle\int_{\Gamma} \frac{e^{ik\rho'\cos(\phi'+t)}\sqrt{1+\cos t}}{\cos t-\cos\phi_{ref}}dt, & \phi' \in (\pi,2\pi) \end{cases} \tag{17}$$

The contour of integration Γ in spectral t-plane (described in the Riemann sheet $\mathrm{Re}\{t\} \in (0,\pi)$) is depicted in Fig. 6. (ρ',ϕ') are the polar coordinates in L-frame described as $x_1' = \rho'\cos\phi'$, $x_2' = \rho'\sin\phi'$.

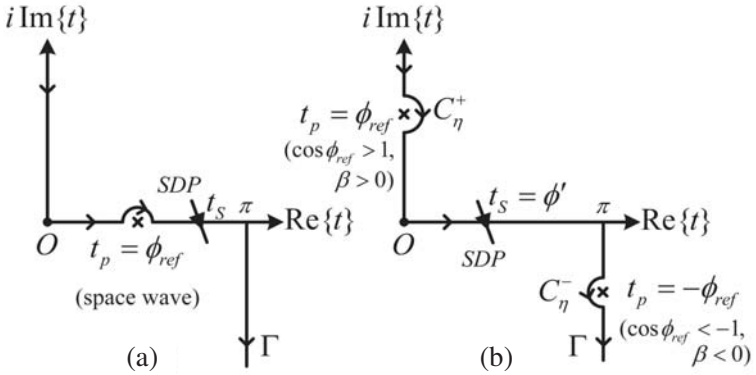

Figure 6. The contour of integration Γ in spectral t-plane in presence of (a) space wave pole, (b) surface wave poles.

It is seen in Eq. (17) that the saddle point always appears in the range $t_s \in (0,\pi)$ on the real axis, while the location of the pole at t_p is dependent on (ϕ_{inc},β).

Case I: $|\cos\phi_{ref}| \leq 1$: Space Wave Scattering

As long as (ϕ_{inc},β) remain in the space wave region (in blue) in Fig. 3(a),

(i) in the reflection region $\phi' \in (0,\phi_{ref})$ the saddle point appears at $t_s = \phi' \in (0,\phi_{ref})$, and therefore, one inevitably crosses over the (space wave) pole while deforming Γ onto the steepest descent path. The residue contribution equals the reflected wave;

(ii) in the region $\phi' \in (\phi_{ref},\pi)$ the saddle point appears at $t_s = \phi' \in (\phi_{ref},\pi)$ so that the pole is not crossed over during the deformation process;

(iii) in the region $\phi' \in (\pi, 2\pi-\phi_{ref})$ the saddle point appears at $t_s = 2\pi-\phi' \in (\phi_{ref},\pi)$ so that the pole is not crossed over during the deformation process;

(iv) in the shadow region $\phi' \in (2\pi-\phi_{ref}, 2\pi)$ the saddle point appears at $t_s = 2\pi-\phi' \in (0,\phi_{ref})$, and therefore, one inevitably crosses over the pole while deforming Γ onto the steepest descent path. The residue contribution cancels with the incident field in that region.

As a result, the total scattered field can be written as

$$u' = u_d' + \begin{cases} R_{TM}e^{ik\rho'\cos(\phi'-\phi_{ref})}, & 0<\phi'<\phi_{ref} \\ 0, & \phi_{ref}<\phi'<2\pi-\phi_{ref} \\ -R_{TM}e^{ik\rho'\cos(\phi'+\phi_{ref})}, & 2\pi-\phi_{ref}<\phi'<2\pi \end{cases} \tag{18}$$

The term $R_{TM}e^{ik\rho'\cos(\phi'-\phi_{ref})}$, $0<\phi'\leq\phi_{ref}$ corresponds to u_{ref}'. The influence of motion brings about non-zero GO component $u_{inc}' - R_{TM}e^{ik\rho'\cos(\phi'+\phi_{ref})}$ in the expression of the total magnetic field in the region $2\pi-\phi_{ref} \leq \phi' < 2\pi$ in L-frame.

The diffracted magnetic field may be calculated from the saddle point contribution as

$$\begin{cases} u'_d \cong D(\pi-\phi_{ref},\phi')\dfrac{e^{ik\rho'}}{\sqrt{k\rho'}}, \quad k\rho' \gg 1 \\ D(\pi-\phi_{ref},\phi') = -\dfrac{e^{i\pi/4}}{\sqrt{2\pi}} R_{TM} \dfrac{\sqrt{1+\cos(\pi-\phi_{ref})}\sqrt{1+\cos\phi'}}{\cos(\pi-\phi_{ref})+\cos\phi'} \end{cases} \tag{19a,b}$$

The uniform asymptotic evaluation of Eq. (18) along the Steepest Descent Path (SDP), which takes finite values at the reflection boundary $\phi' = \phi_{ref}$, reveals the Sommerfeld diffraction coefficient

$$D(k\rho';\pi-\phi_{ref},\phi') = -\frac{e^{i\pi/4}}{2\sqrt{2\pi}} R_{TM} \times \left[\begin{array}{l} \sec\left(\dfrac{\phi'+\phi_{ref}-\pi}{2}\right) F\left(2k\rho'\cos^2\left(\dfrac{\phi'+\phi_{ref}-\pi}{2}\right)\right) \\ +\sec\left(\dfrac{\phi'-\phi_{ref}+\pi}{2}\right) F\left(2k\rho'\cos^2\left(\dfrac{\phi'-\phi_{ref}+\pi}{2}\right)\right) \end{array} \right] \tag{19c}$$

(well known for $\beta = 0$), where $F(z) = -2i\sqrt{z}e^{-iz}\int\limits_{\sqrt{z}}^{\infty} e^{i\eta^2}d\eta$ is a modified Fresnel integral. The scattered electric field in L-frame can be calculated from the field Equations (9a-d). The diffracted field displays a jump discontinuity

$$u'_d\big|_{\phi'=\phi_{ref}+0^-} - u'_d\big|_{\phi'=\phi_{ref}+0^+} = -R_{TM}\, e^{ik\rho'\cos(\phi'-\phi_{ref})}\Big|_{\phi'=\phi_{ref}} = -R_{TM}e^{ik\rho'}$$

which ensures the continuity of total scattered field in Eq. (18) on the reflection boundary. This relation can be seen upon substituting

$$\cos\left(\frac{\phi'+\phi_{ref}-\pi}{2}\right)\Big|_{\phi'=\phi_{ref}+0^\pm} = \sin\phi_{ref}$$

$$\cos\left(\frac{\phi'-\phi_{ref}+\pi}{2}\right)\Big|_{\phi'=\phi_{ref}+0^\pm} = \cos\left(\frac{\pi}{2}+0^\pm\right) = 0^\mp$$

$$F(z) \sim \sqrt{\pi z}e^{-i\pi/4}e^{-iz}, \quad z\to 0$$

$$\sec\left(\frac{\phi'+\phi_{ref}-\pi}{2}\right) F\left(2k\rho'\cos^2\left(\frac{\phi'+\phi_{ref}-\pi}{2}\right)\right)\Big|_{\phi'=\phi_{ref}+0^\pm} = \frac{1}{\sin\phi_{ref}} F\left(2k\rho'\sin^2\phi_{ref}\right)$$

$$\sec\left(\frac{\phi'+\phi_{ref}+\pi}{2}\right) F\left(2k\rho'\cos^2\left(\frac{\phi'+\phi_{ref}+\pi}{2}\right)\right)\Big|_{\phi'=\phi_{ref}+0^\pm}$$

$$= \operatorname{sign}\left(\cos\left(\frac{\phi'-\phi_{ref}+\pi}{2}\right)\right)\Big|_{\phi'=\phi_{ref}+0^\pm} e^{-i\pi/4}\sqrt{2\pi k\rho'} = \mp e^{-i\pi/4}\sqrt{2\pi k\rho'}$$

into Eq. (19) to get

$$u'_d\big|_{\phi'=\phi_{ref}+0^+} = -\frac{e^{ik\rho'}}{\sqrt{k\rho'}}\frac{e^{i\pi/4}}{2\sqrt{2\pi}} R_{TM}\left[\frac{F\left(2k\rho'\sin^2\phi_{ref}\right)}{\sin\phi_{ref}} - e^{-i\pi/4}\sqrt{2\pi k\rho'}\right]$$

$$u'_d\big|_{\phi'=\phi_{ref}+0^-} = -\frac{e^{ik\rho'}}{\sqrt{k\rho'}}\frac{e^{i\pi/4}}{2\sqrt{2\pi}} R_{TM}\left[\frac{F\left(2k\rho'\sin^2\phi_{ref}\right)}{\sin\phi_{ref}} + e^{-i\pi/4}\sqrt{2\pi k\rho'}\right]$$

The surface current density distribution on S can be calculated from Eq. (7b) for $kx'_1 \gg 1$ as $J'_S(x'_1) = 2R_{TM}e^{ikx'_1\cos\phi_{ref}}$, which corresponds to GO currents.

Case II: $|\cos\phi_{ref}| > 1$: Surface Wave Scattering

In this case, the total scattering mechanism constitutes

(i) the edge diffracted field expressed by SDP contribution in Eq. (19), and
(ii) the surface reflected wave calculated by the contributions from the circular indentations $C_\eta^\pm$ in the Cauchy sense.

Accordingly, the total scattered magnetic field can be written as

$$u' = u'_d + u'_{sw}. \tag{20}$$

u'_d has the same representation as in Eq. (19). However, the cosine terms in Eq. (19b) require to be calculated as

$$\sqrt{1+\cos(\pi-\phi_{ref})} = \sqrt{1-\cos\phi_{ref}} = i\sqrt{\cos\phi_{ref}-1}, \quad \cos\phi_{ref} > 1$$

On the other hand, radiation condition requires to pick

$$\sin\phi_{ref} = \begin{cases} +iN, & x'_2 > 0 \\ -iN, & x'_2 < 0 \end{cases} \tag{21a}$$

and

$$R_{TM} = \begin{cases} +\sin\phi_{inc}/(iN), & x'_2 > 0 \\ -\sin\phi_{inc}/(iN), & x'_2 < 0 \end{cases} \tag{21b}$$

in Eq. (19c).

In calculating u'_{sw} for $\cos\phi_{ref} > 1$ over the semi-circle C_η^+, we set $t_p = \phi_{ref} = i\sinh^{-1}N$, $\sin\phi_{ref} = iN$, $t = t_p + \eta e^{i\varphi}$, $dt = i\eta e^{i\varphi}d\varphi$, $\varphi : \pi/2 \to -\pi/2$, and for $\cos\phi_{ref} < -1$ over the semi-circle C_η^-, we set $t_p = -\phi_{ref} = \pi - i\sinh^{-1}N$, $\sin\phi_{ref} = -iN$, $t = t_p + \eta e^{i\varphi}$, $dt = i\eta e^{i\varphi}d\varphi$, $\varphi : \pi/2 \to 3\pi/2$. The results are obtained in the Cauchy sense as $\eta \to 0$ as

$$u'_{sw} = \frac{1}{2}R_{TM} \times \begin{cases} e^{ik\rho'\cos(\phi'-\phi_{ref})}, & \phi' \in (0,\pi) \\ -e^{ik\rho'\cos(\phi'+\phi_{ref})}, & \phi' \in (\pi,2\pi) \end{cases}, \quad \cos\phi_{ref} > 1 \tag{22a}$$

$$u'_{sw} = \frac{1}{2}R_{TM} \times \begin{cases} e^{ik\rho'\cos(\phi'+\phi_{ref})}, & \phi' \in (0,\pi) \\ -e^{ik\rho'\cos(\phi'-\phi_{ref})}, & \phi' \in (\pi,2\pi) \end{cases}, \quad \cos\phi_{ref} < -1 \tag{22b}$$

which is equal to one half of the residue contributions. u'_{sw} can be shaped into the resultant forms

$$u'_{sw} = -\frac{1}{2Ni}\sin\phi_{inc}e^{-Nk\rho'|\sin\phi'|}e^{ik\rho'\cos\phi'\cos\phi_{ref}} \tag{23a}$$
$$\text{for } \cos\phi_{ref} < -1 \ \ \& \ \ \phi' \in (0,\pi) \text{ and } \cos\phi_{ref} > 1 \ \ \& \ \ \phi' \in (\pi,2\pi)$$

$$u'_{sw} = +\frac{1}{2Ni}\sin\phi_{inc}e^{-Nk\rho'|\sin\phi'|}e^{ik\rho'\cos\phi'\cos\phi_{ref}} \tag{23b}$$
$$\text{for } \cos\phi_{ref} < -1 \ \ \& \ \ \phi' \in (\pi,2\pi) \text{ and } \cos\phi_{ref} > 1 \ \ \& \ \ \phi' \in (0,\pi)$$

and can be interpreted as propagating along both $+x'_1$ and $-x'_1$ directions emanating from $x'_1 = 0$ plane.

One observes the far field relation $|u'_{sw}| \ll |u'_d|$ at all points of observation, probably except when $|\sin\phi'| \to 0$, i.e., in a neighborhood of $\phi' = 0, \pi$ where the surface wave behaves as

$$u'_{sw}\big|_{\phi'\to 0^+} = \mp\frac{1}{2Ni}\sin\phi_{inc}e^{ik\rho'\cos\phi_{ref}}, \quad u'_{sw}\big|_{\phi'\to 2\pi^-} = \pm\frac{1}{2Ni}\sin\phi_{inc}e^{ik\rho'\cos\phi_{ref}}$$
$$u'_{sw}\big|_{\phi'\to \pi^+} = \pm\frac{1}{2Ni}\sin\phi_{inc}e^{-ik\rho'\cos\phi_{ref}}, \quad u'_{sw}\big|_{\phi'\to \pi^-} = \mp\frac{1}{2Ni}\sin\phi_{inc}e^{-ik\rho'\cos\phi_{ref}}$$

for $\cos\phi_{ref} < -1$ and $\cos\phi_{ref} > 1$, respectively. It is seen that u'_{sw} takes opposite limit values while approaching at $\phi' = 0, \pi$ from opposite sides. One observes a phase shift of 180^o upon crossing over x'_1-axis. Due to structural symmetry, u'_d and u'_{sw} have symmetric patterns around x'_1-axis.

In this case, the surface current density distribution on S can be calculated from Eq. (7b) for $kx'_1 \gg 1$ as

$$J'_S(x'_1) = \mp\frac{1}{iN}\sin\phi_{inc}e^{ikx'_1\cos\phi_{ref}}.$$

For very small values of β, in virtue of the investigation in the previous section, surface wave mechanism occurs under grazing wave incidence so that one may insert $\cos\phi_{ref} \to \mp(1+2|\beta|)$ as $\phi_{inc} \to 0, \pi$ in Eqs. (19)–(23).

2.11. Evaluation of Diffraction Coefficient

The modified Fresnel integral function in Eq. (19c) can be expressed in terms of Fresnel cosine and sine functions

$$C_1(z)+iS_1(z)=\sqrt{\frac{2}{\pi}}\int_0^z e^{i\eta^2}d\eta,\quad C_1(\infty)+iS_1(\infty)=\frac{1}{2}(1+i)$$

$$C(z)+iS(z)=\int_0^z e^{i\frac{\pi}{2}\eta^2}d\eta=C_1\left(z\sqrt{\frac{\pi}{2}}\right)+iS_1\left(z\sqrt{\frac{\pi}{2}}\right)$$

as

$$\begin{aligned}F(z)&=-2i\sqrt{z}e^{-iz}\int_{\sqrt{z}}^{\infty}e^{i\eta^2}d\eta=-2i\sqrt{z}e^{-iz}\left[\int_0^{\infty}e^{i\eta^2}d\eta-\int_0^{\sqrt{z}}e^{i\eta^2}d\eta\right]\\&=-2i\sqrt{z}e^{-iz}\sqrt{\frac{\pi}{2}}\left[\frac{1+i}{2}-\left[C_1\left(\sqrt{z}\right)+iS_1\left(\sqrt{z}\right)\right]\right]\\&=-2i\sqrt{z}e^{-iz}\sqrt{\frac{\pi}{2}}\left[\frac{1+i}{2}-\left[C\left(\sqrt{\frac{2z}{\pi}}\right)+iS\left(\sqrt{\frac{2z}{\pi}}\right)\right]\right]\end{aligned}\tag{24a}$$

where $z\in\mathbb{C}$ (cf. [19], Sect. 7.3). One may also use the relation

$$C\left(\sqrt{\frac{2z}{\pi}}\right)+iS\left(\sqrt{\frac{2z}{\pi}}\right)=\frac{1+i}{2}\left[1-e^{iz}\,\varpi\left(e^{i\pi/4}\sqrt{z}\right)\right]\tag{24b}$$

to express Eq. (24a) as

$$F(z)=-i\sqrt{\pi z}\,e^{i\pi/4}\,\varpi\left(e^{i\pi/4}\sqrt{z}\right),\quad z\in\mathbb{C}\tag{24c}$$

in terms of the complex Faddeeva function

$$\varpi(z)=e^{-z^2}\mathrm{erfc}\,(-iz)=e^{-z^2}\left[1+\frac{2i}{\sqrt{\pi}}\int_0^z e^{t^2}\,dt\right],\quad z\in\mathbb{C}\tag{24d}$$

Then, the diffraction coefficient reads

$$D(k\rho';\pi-\phi_{ref},\phi')=-\frac{R_{TM}}{2}\sqrt{k\rho'}\times\left[\begin{array}{l}\varpi\left(e^{i\pi/4}\sqrt{2k\rho'}\left|\cos\left(\dfrac{\phi'+\phi_{ref}-\pi}{2}\right)\right|\right)\\+\varpi\left(e^{i\pi/4}\sqrt{2k\rho'}\left|\cos\left(\dfrac{\phi'-\phi_{ref}+\pi}{2}\right)\right|\right)\end{array}\right]\tag{25a}$$

for space wave scattering ($|\cos\phi_{ref}|\le 1$), and

$$D(k\rho';\pi-\phi_{ref},\phi')=-\frac{R_{TM}}{2}\sqrt{k\rho'}\times\left[\begin{array}{l}\varpi\left(e^{i\pi/4}\sqrt{2k\rho'}\cos\left(\dfrac{\phi'+\phi_{ref}-\pi}{2}\right)\right)\\+\varpi\left(e^{i\pi/4}\sqrt{2k\rho'}\cos\left(\dfrac{\phi'-\phi_{ref}+\pi}{2}\right)\right)\end{array}\right]\tag{25b}$$

for surface wave scattering ($|\cos\phi_{ref}|>1$), where we employ Eq. (22) and the related cosine terms are calculated as

$$\cos\left(\frac{\phi'\mp(\pi-\phi_{ref})}{2}\right)=\cos\left(\frac{\pi\mp\phi'}{2}\right)\sqrt{\frac{1}{2}\left(|\cos\phi_{ref}|+1\right)}+i\sin\left(\frac{\pi\mp\phi'}{2}\right)\sqrt{\frac{1}{2}\left(|\cos\phi_{ref}|-1\right)}$$

for $x_2'>0$ ($\phi'\in(0,\pi)$), and as

$$\cos\left(\frac{\phi'\mp(\pi-\phi_{ref})}{2}\right)=\cos\left(\frac{\pi\mp\phi'}{2}\right)\sqrt{\frac{1}{2}\left(|\cos\phi_{ref}|+1\right)}-i\sin\left(\frac{\pi\mp\phi'}{2}\right)\sqrt{\frac{1}{2}\left(|\cos\phi_{ref}|-1\right)}$$

for $x_2' < 0$ ($\phi' \in (\pi, 2\pi)$).

In virtue of the boundary relation in Eq. (7b), it is expected that

$$D(k\rho'; \pi - \phi_{ref}, \phi')\big|_{\phi' \to 0^+} \neq D(k\rho'; \pi - \phi_{ref}, \phi')\big|_{\phi' \to 2\pi^-}$$

This can be confirmed based on the general property

$$\varpi(z) \neq \varpi(-z), \quad z \in \mathbb{C}$$

where $z = e^{i\pi/4}\sqrt{2k\rho'}\sin(\phi_{ref}/2)$ in this particular case.

In the presence of space waves, one may obtain the first order asymptotic behavior of Faddeeva function for (real valued) large arguments as

$$\varpi\left(e^{i\pi/4}\sqrt{z}\right) \simeq \sqrt{\frac{2}{\pi}}\frac{e^{-iz}}{e^{i\pi/4}\sqrt{z}}\left[\cos\left(z+\frac{\pi}{4}\right) + i\cos\left(z-\frac{\pi}{4}\right)\right], \quad z \to \infty$$

upon inserting the corresponding well-known asymptotic behaviors of Fresnel sine and cosine functions,

$$C(z) \simeq \frac{1}{2} - \frac{\sqrt{2}}{\pi z}\cos\left(\frac{\pi}{2}z^2 + \frac{\pi}{4}\right), \quad z \to \infty, \qquad S(z) \simeq \frac{1}{2} - \frac{\sqrt{2}}{\pi z}\cos\left(\frac{\pi}{2}z^2 - \frac{\pi}{4}\right), \quad z \to \infty$$

into Eq. (23b). This reveals that the pattern of $|D|$ in Eq. (25a) is loosely dependent on electrical distance $k\rho'$ in the far field.

The far field pattern of $|D|$ in Eq. (25b) can be estimated employing the asymptotic behavior of Faddeeva function with complex arguments [20]

$$\varpi(z) \sim \frac{i}{\sqrt{\pi}z}\left(1 + \sum_{n=1}^{\infty}\frac{(2n-1)!!}{(2z^2)^n}\right), \quad \mathrm{Re}\{z\} \leq -10.$$

Symmetric parameters (ϕ_{inc}, β) and $(\pi - \phi_{inc}, -\beta)$ generate same amplitude patterns for u_d' and u_{sw}'.

2.12. Far Field Scattered Wave in E-Frame

The resultant expression of the scattered magnetic field in E-frame can be obtained as

$$\begin{cases} \vec{H}_d(\vec{r}; t) = \hat{x}_3\,\mathrm{Re}\left\{u_d(x_1, x_2; t)e^{-i\omega_{ref}' t}\right\} \\ \vec{H}_{sc}(\vec{r}; t) = \hat{x}_3\,\mathrm{Re}\left\{u(x_1, x_2; t)e^{-i\omega_{ref}' t}\right\} \end{cases} \tag{26a}$$

upon substituting

$$u_d(x_1, x_2; t) = u_d'\big|_{\substack{\rho' \to \bar{\rho} \\ \phi' \to \bar{\phi}}}, \quad u(x_1, x_2; t) = u'\big|_{\substack{\rho' \to \bar{\rho} \\ \phi' \to \bar{\phi}}} \tag{26b}$$

where

$$\bar{\rho} = \sqrt{(x_1 - Gt)^2 + x_2^2}, \quad \bar{\phi} = \tan^{-1}\left[x_2/(x_1 - Gt)\right] \tag{27}$$

3. MOTION PERPENDICULAR TO THE PLANE

In this mode, the velocity vector and Galilean Transformations are expressed by $\vec{\mathrm{v}} = \hat{x}_2 G$, $G = \mathrm{const.}$ and

$$x_1 = x_1', \quad x_2 = x_2' + Gt, \quad x_3 = x_3', \quad i = 1, 2, 3.$$

For an L-observer located on the PEC half-plane, the velocity field of the ambient medium $\mathbb{R}_3 \backslash S$ and the angular frequency of the incoming wave are observed as

$$\vec{\mathrm{v}}\,' = -\hat{x}_2' G \quad \text{and} \quad \omega_{inc}' = \omega_{inc}(1 + \beta\sin\phi_{inc}).$$

The condition

$$\omega_{inc}' > 0 \quad \text{i.e.,} \quad 1 + \beta\sin\phi_{inc} > 0 \tag{28}$$

appears as the first kinematic requirement on (ϕ_{inc}, β) for the realization of wave reflection phenomenon.

Then, the BVP in Eq. (12) uniquely reads

$$\phi_{ref} = \phi^0_{ref} = \pi - \phi_{inc} \tag{29a}$$

$$\omega'_{ref} = \omega_{inc}(1 + \beta \sin\phi_{ref}) = \omega_{inc}(1 + \beta \sin\phi_{inc}) \tag{29b}$$

$$R_{TM} = \sin\phi_{inc} / \sin\phi_{ref} = 1, \tag{29c}$$

and Eq. (29a) reveals that no surface wave excitation is observed in this mode. Again, in TE mode the angle and frequency of the reflected wave are the same as in TM mode with $R_{TE} = -1$.

The angular frequency of the reflected wave as observed in E-frame is obtained as

$$\omega_{ref} = \omega_{inc}(1 + 2\beta \sin\phi_{inc}). \tag{29d}$$

Equation (29d) reveals the well-known Doppler Effect due to the component of the incident wave parallel to the direction of motion. When we express the angular frequency of the reflected wave as $\omega_{ref} = \omega_{inc} + \Delta\omega$, we get

$$\Delta\omega/\omega_{inc} = 2\beta \sin\phi_{inc}.$$

One observes that $\Delta\omega \geq 0$ when $\beta \geq 0$, and $\Delta\omega \leq 0$ when $\beta \leq 0$.

The condition in Eq. (28) is satisfied provided that $\omega_{ref} > 0$ i.e., $1 + 2\beta \sin\phi_{inc} > 0$, which addresses the permissible region illustrated in Fig. 7 for $\beta < 0$.

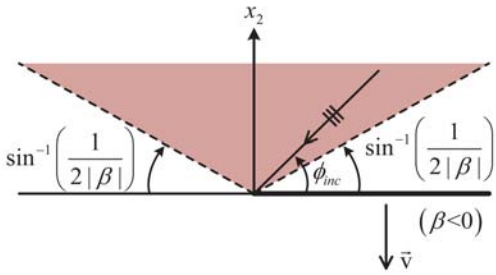

Figure 7. Variation of (painted) range of ϕ_{inc} with $\beta < 0$ in which wave phenomena is realized for uniform motion perpendicular to the plane.

The diffracted magnetic fields in L- and E-frames have the same expressions as in Eqs. (19) and (26) for the kinematic transformations in Eq. (27) are now replaced by

$$\rho' \to \bar{\rho} = \sqrt{x_1^2 + (x_2 - Gt)^2}, \quad \phi' \to \bar{\phi} = \tan^{-1}\left[(x_2 - Gt)/x_1\right]$$

4. NUMERICAL RESULTS

We shall provide the numerical results in L-frame and only for parallel motion as the numerical values of the phasor fields in the other mode are identical with the stationary case. In computations we use Faddeeva.m file written by Abrarov and Quine in [21] for calculating Eq. (24d), which works with accuracy over 1e-13 in entire complex plane.

The mechanism of diffraction of space waves is investigated for 4 combinations of (ϕ_{inc}, β):

- Case I_1 : $\phi_{inc} \in (0, \pi/2)$ $\beta < 0$
- Case I_2 : $\phi_{inc} \in (\pi/2, \pi)$ $\beta < 0$
- Case I_3 : $\phi_{inc} \in (0, \pi/2)$ $\beta > 0$
- Case I_4 : $\phi_{inc} \in (\pi/2, \pi)$ $\beta > 0$

The following evidences are common in all cases:

(i) The shadow region $2\pi - \phi^0_{ref} < \phi' < 2\pi$ in stationary case disappears in the presence of motion. This is due to the presence of non-zero GO field $u'_{inc} - R_{TM} e^{ik\rho' \cos(\phi' + \phi_{ref})}$ in that region.

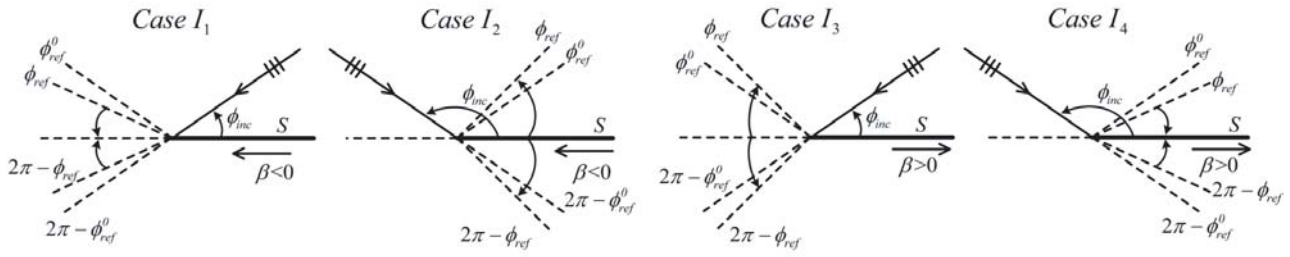

Figure 8. Bending mechanism of diffraction patterns in the directions of curved arrows upon motion.

(ii) The diffraction pattern narrows in Case I_1 and Case I_4 (and widens in Case I_2 and Case I_3) while intensifying in each case with $|\beta|$ as sketched in Fig. 8. The amplification is relatively higher around the shadow boundary as the incidence is from upper half-space. Due to reciprocity, Case I_1 vs. Case I_4 and Case I_2 vs. Case I_3 have mirror symmetric diffraction coefficients.

These evidences are illustrated in Figs. 9–10 for mechanisms I_1 and I_2 over the polar patterns of $|D(k\rho';\phi_{ref},\phi')|$ and the total magnetic field $|u'_{tot}| = |u'_{inc}+u'|$ in dB at $k\rho' = 20\pi$ for $\phi' \in (0, 2\pi)$. One may observe the jump discontinuity for $\phi' = 0$, which is proportional to the amount of surface current density on the half-plane.

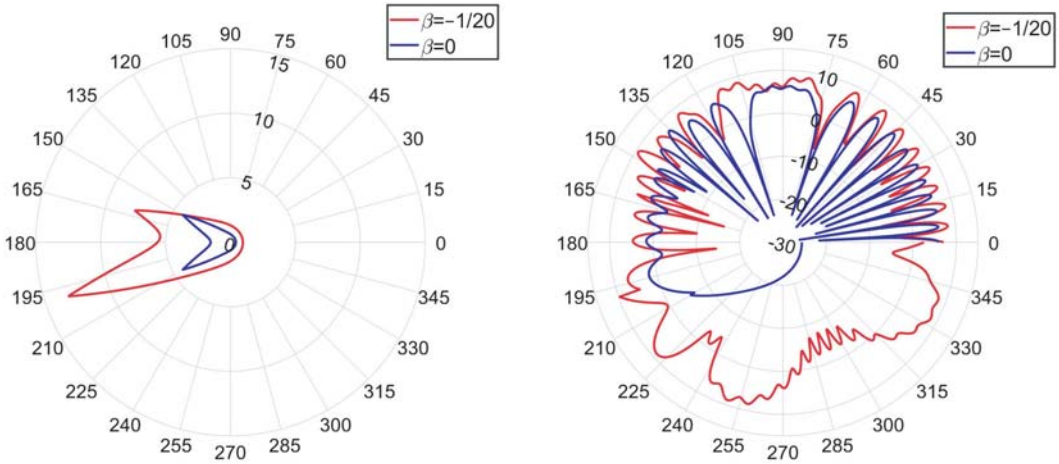

Figure 9. Case I_1: (a) $|D(k\rho' = 20\pi; \phi_{ref} = 161.47°, \phi')|$ for $\beta = 0$ and $\beta = -1/20$ with $\phi_{inc} = 30°$, (b) total field $|u'_{tot}|$ in dB for $(\phi_{inc}, \beta) = (30°, -1/20)$ at $k\rho' = 20\pi$.

The increase of $|D|$ with $|\beta|$ is related with the contribution of the momentum of the PEC plane to scattering mechanism. However, this effect is not much visible until β reaches values comparable to 1.

Similar considerations hold for the case of TE polarization.

With regard to diffraction of surface waves, in Fig. 11 the relative contributions of the constituents of the total diffracted field, $|u'_d|$ and $|u'_{sw}|$ in [dB], are illustrated when $(\phi_{inc}, \beta) = (30°, -0.1)$ with $\cos\phi_{ref} < -1$ (corresponding to Case II_1) at different values of electrical distance (in the far field). As expected, the exponentially decaying nature of the surface reflected wave along x'_2-axis in Eq. (23) exhibits itself as $|u'_{sw}| \ll |u'_d|$ at all points of observation except in a neighborhood of $\phi' = 0, \pi$, which narrows with increasing values of $k\rho'$. The same individual patterns for $|u'_d|$ and $|u'_{sw}|$ are to be observed for the symmetric parameters $(\phi_{inc}, \beta) = (150°, 0.1)$ with $\cos\phi_{ref} > 1$.

In Fig. 12, the total magnetic field $u'_{tot} = u'_{inc} + u'_{sw} + u'_d$ is illustrated in dB at different values of electrical distance (in the far field) for $(\phi_{inc}, \beta) = (30°, -0.1)$. The jump discontinuity at $\phi' = \pi$ is

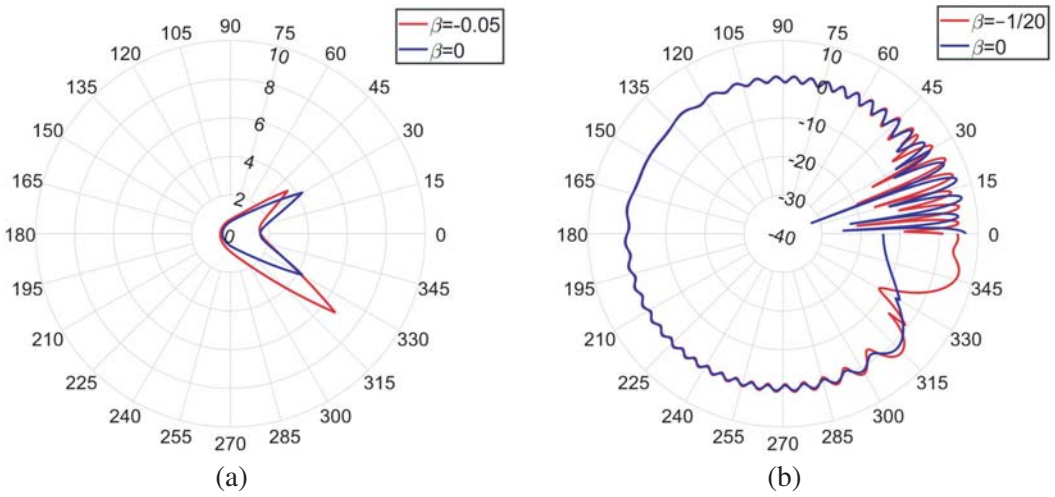

(a) (b)

Figure 10. Case I_2: (a) $|D(k\rho' = 20\pi; \phi_{ref} = 37.15^\circ, \phi')|$ for $\beta = 0$ and $\beta = -1/20$ with $\phi_{inc} = 150^\circ$, (b) total field $|u'_{tot}|$ in dB for $(\phi_{inc}, \beta) = (30^\circ, -1/20)$ at $k\rho' = 20\pi$.

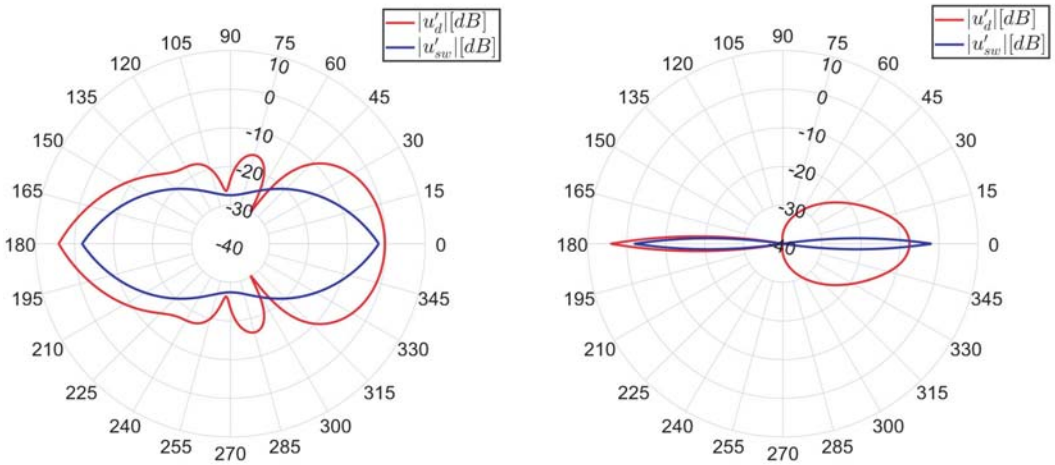

(a) (b)

Figure 11. $|u'_d|$ vs. $|u'_{sw}|$ in dB for $(\phi_{inc}, \beta) = (30^\circ, -1/10)$ at (a) $k\rho' = 3\pi$, (b) $k\rho' = 30\pi$.

observed for the total magnetic field. The contribution of the surface wave is visible as $\phi' \to \pi^{\pm}$, while the total field decreases gradually with $k\rho'$ in all directions.

5. A COMPARISON WITH RELATIVISTIC APPROACH

In [22], the same problem is investigated using Special Relativity Theory (SRT). HE and SRT belong to two separate world views with contradicting predictions. In Table 2, we outline a conceptual comparison of Classical vs. Relativistic Continuum Mechanics to display the contrast in the terminologies of these two world views.

The essential discrepancy rests on the fact that the Lorentz Transformations (in $\mathbb{R}_1$)

$$x' = \gamma\,(x - Gt)\,, \quad t' = \gamma\,(t - \beta x/c) \quad \text{with} \quad \gamma = 1/\sqrt{1-\beta^2} \tag{30a}$$

reduce into

$$x' = x - Gt, \quad t' = t - \beta x/c \tag{30b}$$

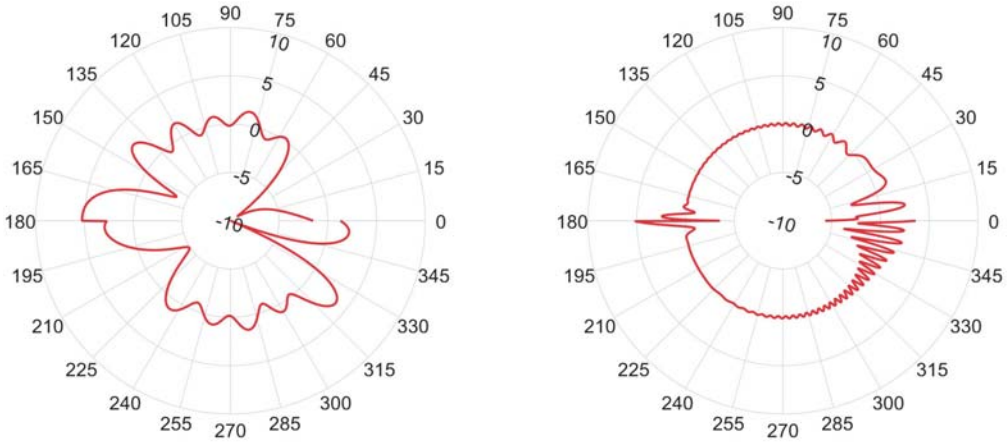

Figure 12. $|u'_{tot}|$ in dB for $(\phi_{inc}, \beta) = (30°, -1/10)$ at (a) $k\rho' = 3\pi$, (b) $k\rho' = 30\pi$.

Table 2. A terminological comparison of the concepts of classical and relativistic continuum mechanics.

Classical Continuum Mechanics	vs.	**Relativistic Continuum Mechanics**
General invariance	vs.	General covariance
Frame indifference	vs.	Form invariance
Newtonian space-time	vs.	Minkowski space-time
Euclidean transformations	vs.	Lorentz transformations
Principle of Material Frame Indifference	vs.	Principle of General Space-Time Covariance
Hertz-Heaviside Electrodynamics (1893)	vs.	Maxwell-Minkowski Electrodynamics (1908) & General Relativity Theory (1916)

under a first order approximation in β, which does not coincide with Galilean transformations

$$x' = x - Gt, \quad t' = t. \tag{31}$$

The contrast between Eqs. (30b) and (31) indicates that at least a first (sometimes higher) order departure in β should be expected between the predictions of HE and SRT in any scenario. In the context of our current investigation, these contradicting predictions can be seen clearly by comparing the physical and geometrical quantities of the space reflected waves for these two theories as outlined in Tables 3 and 4. The results related to SRT can be checked from ([23], Ch. 5) and the references cited therein.

In parallel motion mode, SRT predicts no Doppler shift, unlike HE. One observes a first order departure in β between the results calculated by these two methods.

In perpendicular motion mode, HE predicts that the angle of reflection is unaffected by motion, unlike SRT which indicates an aberration with a first order departure in β between the two results. On the other hand, both methods predict a Doppler shift, while the departure in between the corresponding results is of order β^2.

Nevertheless, the evidences of these two theories for the present problem share common motives as

(i) nonharmonic nature of diffracted fields in E-frame,

(ii) dependence of reflection and shadow boundaries on motion,

(iii) disappearance of shadow region upon motion,

(iv) intensifying of scattered field upon motion due to energy/momentum transfer.

Table 3. A comparison of the results derived with HE and SRT for reflection from a PEC plane for motion parallel to the plane.

Solution by HE	**Solution by SRT**
$R_{TE}=-1,\ R_{TM}=\sin\phi_{inc}/\sin\phi_{ref}$	$R_{TE/TM}=\mp 1$
$\dfrac{\cos\phi_{ref}}{\cos(\pi-\phi_{inc})}=\dfrac{\omega_{ref}}{\omega_{inc}}=\dfrac{1}{1+2\beta\cos\phi_{inc}}$	$\phi_{ref}=\pi-\phi_{inc},\ \omega_{ref}=\omega_{inc}$ No Doppler shift
$\left(\dfrac{\cos\phi_{ref}}{\cos(\pi-\phi_{inc})}\right)_{HE}-\left(\dfrac{\cos\phi_{ref}}{\cos(\pi-\phi_{inc})}\right)_{SRT}=\left(\dfrac{\omega_{ref}}{\omega_{inc}}\right)_{HE}-\left(\dfrac{\omega_{ref}}{\omega_{inc}}\right)_{SRT}=-2\beta\cos\phi_{inc}+\text{h.o.t. in }\beta$	

Table 4. A comparison of the results derived with HE and SRT for reflection from a PEC plane for motion perpendicular to the plane.

Solution by HE	**Solution by SRT**
$R_{TE/TM}=\mp 1,\ \phi_{inc}=\pi/2$	$R_{TE/TM}=\mp(1-\beta)/(1+\beta),\ \phi_{inc}=\pi/2$
$\phi_{ref}=\pi-\phi_{inc},\ \sin\phi_{ref}=\sin\phi_{inc}$ $\dfrac{\omega_{ref}}{\omega_{inc}}=1+2\beta\sin\phi_{inc}$	$\sin\phi_{ref}=\dfrac{(1+\beta^2)\sin\phi_{inc}-2\beta}{1-2\beta\sin\phi_{inc}+\beta^2}$ $\dfrac{\omega_{ref}}{\omega_{inc}}=\dfrac{1-2\beta\sin\phi_{inc}+\beta^2}{1-\beta^2}=\dfrac{1-\beta\sin\phi_{inc}}{1+\beta\sin\phi_{ref}}$
$(\sin\phi_{ref}-\sin\phi_{inc})_{HE}-(\sin\phi_{ref}-\sin\phi_{inc})_{SRT}=2\beta\cos^2\phi_{inc}+\text{h.o.t. in }\beta$ $(\omega_{ref}/\omega_{inc})_{HE}-(\omega_{ref}/\omega_{inc})_{SRT}=2\beta^2+\text{h.o.t in }\beta$ $\big(R_{TE/TM}\big)_{HE}-\big(R_{TE/TM}\big)_{SRT}=\mp 2\beta+\text{h.o.t. in }\beta,\ \phi_{inc}=\pi/2$	

6. CONCLUSION

Scattering of homogeneous plane waves by a Perfect Electric Conductor half-plane in uniform rectilinear motion in a simple lossless medium is investigated using Wiener-Hopf Technique in the context of Hertzian Electrodynamics. Numerical results are illustrated and discussed for scattered fields. The methodology is planned to be extended to PEC and impedance half-planes with different modes of motion, such as uniform rectilinear acceleration, rotation, and oscillation in virtue of the available results [15, 16] for a PEC plane and later to rotating strips in conjunction with novel analytical micro-Doppler analyses of electromagnetic modulation due to rotor blades and wind turbines. Availability of the explicit expression of the diffraction coefficient in the presence of motion and similarity of its analytical structure to stationary case are also encouraging for extending existing asymptotic ray techniques for RCS and maneuver predictions of moving targets.

HFE can be interpreted as an enhancement of Maxwell equations of stationary with the Lie derivative operator, whose analytical properties are summoned up in [11]. In this manner, it is possible to fully characterize the influence of all modes of motion in any macroscobic electromagnetic phenomenon. This is equivalent to saying that moving media problems cannot be correctly formulated upon Maxwell equations by incorporating time only as a parameter that specifies the instantaneous location of a moving medium. This can be seen directly upon formulating the reflection of an oblique incident plane wave from a moving PEC surface as the Maxwell formulation shall only reveal the Snell's law of stationary media. A similar comparison of true Hertzian formulation [15] versus Maxwell formulation [24] can be done for the problem of reflection by a PEC plane in harmonic motion.

Finally, we should emphasize that relativistic formulations are not relevant to moving media

problems in the context of Electrical Engineering. In that regard, we should draw attention to the literature which invalidates the relativistic Doppler shift [25–28] and relativistic GPS corrections [29] in comparison to the classical (Hertzian) theory.

ACKNOWLEDGMENT

This work was supported by Research Fund of the Yildiz Technical University. Project Number: FDK-2019-3680.

REFERENCES

1. Hertz, H., "Über die Grundgleichungen der Elektrodynamik für bewegte Körper," *Annalen der Physik*, Vol. 41, 369–399, 1890.
2. Heaviside, O., "The Electrician," *Electromagnetic Theory*, Vol. 1, Printing and Publishing Company Ltd., 1893.
3. Truesdell, C. and R. Toupin, *The Classical Field Theories. In: Flügge, S. (ed.) Prinzipien der klassischen Mechanik und Feldtheorie*, Vol. 2, 226–793, Handbuch der Physik, Springer, 1960.
4. Truesdell, C. and W. Noll, *The Non-linear Field Theories of Mechanics*, 3rd Edition, Springer, 1965.
5. Frewer, M., "More clarity on the concept of material frame-indifference in classical continuum mechanics," *Acta Mech*, Vol. 202, 213–246, 2009.
6. Christov, C. I., "On the analogy between the Maxwell electromagnetic field and the elastic continuum," *Annuaire de L'Universite de Sofia*, Vol. 95, 109–121, 2001.
7. Christov, C. I., "On the material invariant formulation of Maxwell's displacement current," *Foundations of Physics*, Vol. 36, No. 11, 1701–1717, 2006.
8. Christov, C. I., "On the nonlinear continuum mechanics of space and the notion of luminiferous medium," *Nonlinear Analysis: Theory, Methods & Applications*, Vol. 71, No. 12, e2028–e2044, 2009.
9. Christov, C. I., "Frame indifferent formulation of maxwell's elastic fluid model and the rational continuum mechanics of the electromagnetic field," *Mechanics Research Communications*, Vol. 38, No. 4, 334–339, 2011.
10. Oldroyd, J. G., "On the formulation of rheological equations of state," *Proceedings of the Royal Society of London. Series A. Mathematical and Physical Sciences*, Vol. 200, No. 1063, 523–541, 1950.
11. Polat, B., "On the axiomatic structure of hertzian electrodynamics," *TWMS Journal of Applied and Engineering Mathematics*, Vol. 2, No. 1, 17–41, 2012.
12. Polat, B., "Scattering by a moving PEC plane and a dielectric half-space in hertzian electrodynamics," *TWMS Journal of Applied and Engineering Mathematics*, Vol. 2, No. 2, 123–144, 2012.
13. Polat, B., "Scattering by a moving circular cylinder in hertzian electrodynamics," *Selçuk Journal of Applied Mathematics*, Vol. 13, No. 1, 89–109, 2012.
14. Polat, B. and R. Daşbaşı, "Validation of hertzian electromagnetism in a rectangular waveguide with rotating PEC termination," *2019 PhotonIcs & Electromagnetics Research Symposium — Spring (PIERS-Spring)*, 2850–2856, Rome, Italy, 2019, doi: 10.1109/PIERS-Spring46901.2019.9017394.
15. Polat, B. and R. Daşbaşı, "Plane wave reflection by a PEC plane in harmonic motion," *2020 International Conference on Electrical, Communication, and Computer Engineering (ICECCE)*, 1–6, Istanbul, Turkey, Jun. 12–13, 2020, doi: 10.1109/ICECCE49384.2020.9179436.
16. Polat, B. and R. Daşbaşı, "Hertzian formulation of scattering by moving PEC bodies," *IEEE Microwaves, Radar and Remote Sensing Symposium (MRRS-2020)*, Kharkiv, Ukraine, Sept. 21–25, 2020.

17. Polat, B. and R. Daşbaşı, "On conservation of electromotive force in hertzian electrodynamics," *2020 International Conference on Electrical, Communication, and Computer Engineering (ICECCE)*, 1–6, Istanbul, Turkey, Jun. 12–13, 2020, doi: 10.1109/ICECCE49384.2020.9179200.
18. Noble, B., *Methods Based on the Wiener-Hopf Technique for the Solution of Partial Differential Equations*, Pergamon Press, 1958.
19. Abramowitz, M. and I. A. Stegun, *Handbook of Mathematical Functions with Formulas, Graphs, and Mathematical Tables*, Dover Publications, 1974.
20. Poppe, G. P. M. and C. M. J. Wijers, "More efficient computation of the complex error function," *ACM Transactions on Mathematical Software*, Vol. 16, No. 1, 38–46, 1990.
21. Abrarov, S. M., B. M. Quine, and R. K. Jagpal, "A sampling-based approximation of the complex error function and its implementation without poles," *Applied Numerical Mathematics*, Vol. 129, 181–191, 2018.
22. Idemen, M. and A. Alkumru, "Relativistic scattering of a plane wave by a uniformly moving half-plane," *IEEE Transactions on Antennas and Propagation*, Vol. 54, No. 11, 3429–3440, 2006.
23. Van Bladel, J., *Relativity and Engineering*, Springer-Verlag, 1984.
24. Borkar, S. and R. F. Yang, "Reflection of electromagnetic waves from oscillating surfaces," *IEEE Transactions on Antennas and Propagation*, Vol. 23, No. 1, 122–127, 1975.
25. Pobedonostsev, L. A., "Experimental studies of the Doppler effect," *Journal of Systems Engineering and Electronics*, Vol. 6, No. 4, 115–128, 1995.
26. Thim, H. W., "Absence of the relativistic transverse Doppler shift at microwave frequencies," *IEEE Transactions on Instrumentation and Measurement*, Vol. 52, No. 5, 1660–1664, 2003.
27. Sfarti, A. "Comment on "The case of absence of transverse Doppler effect"," *IEEE Transactions on Instrumentation and Measurement*, Vol. 59, No. 2, 494–495, 2010, doi: 10.1109/TIM.2009.2034324.
28. Thim, H., "Response: The case of absence of transverse Doppler effect," *IEEE Transactions on Instrumentation and Measurement*, Vol. 59, No. 2, 495–495, 2010, doi: 10.1109/TIM.2009.2034326.
29. Hatch, R. R., *Escape from Einstein*, 1st Edition, Kneat Kompany, 1992.